Dalton Transactions

Accepted Manuscript

ROYAL SOCIETY OF CHEMISTRY

www.rsc.org/dalton

Journal Name

RSCPublishing

ARTICLE

Crystal Structures, CO_2 Adsorption, and Dielectric Properties of $[Cu(II)_2(R\text{-Benzoate})_4(pyrazine)]_\infty$ Polymers (R = *m*-F, 2,3-F_2, *m*-Cl, and *m*-CH_3)

Cite this: DOI: 10.1039/x0xx00000x

Received 00th January 2012,
Accepted 00th January 2012

DOI: 10.1039/x0xx00000x

www.rsc.org/

Kiyonori Takahashi,[a] Norihisa Hoshino,[a, b] Takashi Takeda,[a, b] Shin-ichiro Noro,[c] Takayoshi Nakamura,[c] Sadamu Takeda,[d] and Tomoyuki Akutagawa*[a, b]

m-Fluorobenzoate (*m*-FBA), 2,3-difluorobenzoate (2,3-F_2BA), *m*-methylbenzoate (*m*-MBA), and *m*-chlorobenzoate (*m*-ClBA) were introduced into the Cu(II) binuclear unit as bridging ligands between two Cu(II) sites, which were further connected by an axial pyrazine (pz) ligand to form one-dimensional coordination polymers of $[Cu(II)_2(m\text{-FBA})_4(pz)]_\infty$ (**1**), $[Cu(II)_2(2,3\text{-}F_2BA)_4(pz)]_\infty$ (**2**), $[Cu(II)_2(m\text{-MBA})_4(pz)]_\infty$ (**3**), and $[Cu(II)_2(m\text{-ClBA})_4(pz)]_\infty$ (**4**), respectively. The parallel arrangements of one-dimensional (1D) polymers results in 1D channels between the polymers that crystallization CH_3CN molecules can occupy to form single crystals of **1**•4CH_3CN, **2**•4CH_3CN, **3**•2CH_3CN, and **4**•2CH_3CN. Both π-dimer and dipole-dipole interactions were simultaneously observed in the interchain interactions of *m*-FBA and/or 2,3-F_2BA ligands in crystals **1** and **2**. The sizes of the one-dimensional channels between the polymers are thus modulated according to the interchain interactions between the polar BA ligands. CH_3CN molecules within the channels were easily replaced by H_2O under ambient conditions. CO_2 adsorption-desorption isotherms of crystals **1**, **2**, and **3** at 195 K indicated gate-adsorption with a hysteresis, whereas two-step gate-adsorption behavior was observed for CO_2 in crystal **4**. Temperature- and frequency-dependent dielectric responses were not observed in crystals **1**-**4** under vacuum conditions, whereas dielectric anomalies were observed around 290 K for crystals **1** and **2** with adsorbed CO_2. CO_2 desorption from the channels in crystals **1** and **2** activated the molecular motions of polar BA ligands and dielectric responses around 290 K, which were confirmed by CO_2 adsorption-desorption isotherms around 290 K and differential scanning calorimetries under CO_2 condition.

Introduction

A variety of metal-organic-frameworks (MOFs) have been designed to realize crystalline environments for phenomena such as selective gas adsorption-desorption, organic reactions, and proton transport.[1-3] The network structures of MOFs are constructed from the coordination geometries between the metal and organic ligands, which results in a variety of structural modifications through the design of the organic ligands. One-dimensional metal coordination polymers are one type of structural unit used to design physical properties such as electrical conduction, magnetism, and non-linear optical properties.[4-6] Among these, the one-dimensional magnets have been extensively examined in $Co^{II}(hfac)_2$(NITPhOMe) (hfac = hexafluoroacetylacetonate, NITPhOMe = 4'-methoxy-phenyl-4,4,5,5-tetramethylimidazoline-1-oxyl-3-oxide), and $[Mn_2(saltmen)_2Ni(pao)_2(py)_2](ClO_4)_2$ (saltmen^{2-} = *N*,*N*'-(1,1,2,2-tetramethylethylene)bis(salicylideneiminate), pao$^-$ = pyridine-2-aldoximate, py = pyridine) through the chemical design of intrachain interactions.[5] High electrical conduction has been reported in mixed-valence coordination complexes such as metal(phthalocyanines), metal-halogen (MX) chains, and partailly oxidaized $[Ni(dmit)_2]$ crystals (dmit = 2-thioxo-1,3-dithiole-4,5-dithiolate).[6-8] The design of the *d*-orbital energy levels of the transition metal and the π-orbitals of organic ligands enable a variety of electrical conduction, magnetic, and optical properties. In the one-dimensional systems, interchain interactions between the polymers play an important role to determine the bulk physical properties. For instance, the quantum magnetic behavior of single chain magnets disappears with an increase in interchain interactions,[9] and the metal-insulator transition is suppressed by an increase in the interchain interactions.[10]

Among the variety of one-dimensional coordination polymers, the selective gas-adsorption and structural phase transition behaviors of paddle-wheel type $[Cu(II)_2(BA)_4(pz)]_\infty$ and $[Rh(II)_2(BA)_4(pz)]_\infty$ (BA = benzoate, and pz = pyrazine) polymers have been extensively examined by Takamizawa et al.[11] The two metal ion sites are coordinated by the oxygen atoms of four BA ligands, which are further connected by the nitrogen sites of the axial pz ligands. It should be noted that the structural phase transitions coupled with the gas adsorption-desorption properties are observed for single crystal $[Rh(II)_2(BA)_4(pz)]_\infty$. A variety of molecules such as CO_2, H_2, O_2, N_2, Ar, and C_2H_5OH can pass through the one-dimensional channels between the polymers, where the gas transport properties within the single crystals are achieved by structural design of the intrachain and interchain interactions. In addition, the BA and pz ligands in the $[Cu(II)_2(BA)_4(pz)]_\infty$ crystal exhibit dynamic characteristics, such as the two-fold flip-flop motion of the BA and pz ligands, as observed by room temperature solid-state ^{1}H nuclear magnetic spectroscopy

(NMR) and ^{2}H NMR. When the structural phase transition and molecular motion of polar units are coupled to each other, huge dielectric responses are expected in the solid state. The gas adsorption-desorption properties of the $[Cu(II)_2(BA)_4(pz)]_\infty$ crystal are associated with the motional freedom of the ligands, so that coupling between gas adsorption, molecular motion, and the dielectric response has the potential to realize multifunctional molecular materials.

Although the two-fold flip-flop motions of BA and pz ligands are observed in the $[Cu(II)_2(BA)_4(pz)]_\infty$ crystal, the dielectric responses are not affected by these molecular motions, because the same molecular structures are present with the initial and rotated states. We have reported the solid-state molecular rotators of anilinium (Ani^+) and adamantylammonium ($ADNH_3^+$) in (Ani^+)([18]crown-6)[Ni(dmit)$_2$] and ($ADNH_3^+$)([18]crown-6)[Ni(dmit)$_2$] crystals (dmit = 2-thioxo-1,3-dithiole-4,5-dithiolate).[12] The rotations of the Ani^+ and $ADNH_3^+$ cations along the C-NH_3^+ axis have two-fold and three-fold symmetries, respectively, which are dominated by the molecular structures of the rotators. However, the rotations of the Ani^+ and $ADNH_3^+$ cations did not have a significant influence on the physical properties of the crystals, such as the magnetic and dielectric properties. In contrast, the two-fold flip-flop motion of the *m*-fluoroanilinium (*m*-$FAni^+$) cation along the C-NH_3^+ axis in the (*m*-$FAni^+$)(dibenzo[18]crown-6)[Ni(dmit)$_2$] crystal resulted in a ferroelectric-paraelectric phase transition at 348 K.[13] The dipole inversion could be achieved by the two-fold flip-flop motion of the *m*-$FAni^+$ cation due to different molecular structures for the initial and rotated states. Huge dielectric responses were activated by the thermal molecular motions of ligands in the $[Cu(II)_2$(adamantane carboxylate)$_4$(DMF)$_2$]•$(DMF)_2$ crystal (DMF = *N*, *N*′-dimethylformamide), where the thermally activated rotation of adamantyl-groups was coupled with the molecular motions of polar DMF.[14] The molecular motions of crystallization DMF molecules in the one-dimensional channel resulted in huge frequency- and temperature-dependent dielectric responses around 270 K.[14] Although the spherical adamantyl-groups are useful to construct rotary units in a crystalline environment, rotary ligands with polar substituents are necessary to realize dielectric responses. Therefore, we have considered Cu(II) coordination polymers with polar ligands of *m*-fluorobenzoate (*m*-FBA), 2,3-difluorobenzoate (2,3-F_2BA), *m*-methylbenzoate (*m*-MBA), and *m*-chlorobenzoate (*m*-ClBA). Four new polymer crystals of $[Cu(II)_2$(*m*-FBA)$_4(pz)]_\infty$ (**1**), $[Cu(II)_2$(2,3-F_2BA)$_4(pz)]_\infty$ (**2**), $[Cu(II)_2$(*m*-MBA)$_4(pz)]_\infty$ (**3**), and $[Cu(II)_2$(*m*-ClBA)$_4(pz)]_\infty$ (**4**) were prepared, where Cu(II) binuclear units with polar BA ligands were connected through the axial ligand of pz to form one-dimensional polymers (Scheme 1). The crystal structures, CO_2 adsorption-desorption isotherms, and dielectric responses of these crystals under CO_2 were evaluated with respect to the interchain interactions.

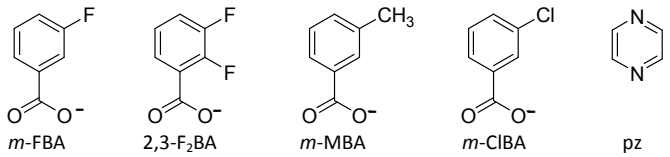

Scheme 1. Molecular structures of four types of BA and pz ligands in Cu(II) coordination polymers **1**–**4**.

Experimental Section

Preparation. Commercially available *m*-FBA, 2,3-F_2BA, *m*-MBA, and *m*-ClBA were employed for crystal growth without further purification. Single crystals **1**-**4** were prepared by the slow diffusion method in CH_3CN using an H-shaped cell (50 mL). $[Cu(OAc)_2]•H_2O$ (2×10^{-4} mol) and the corresponding BA ligand (10×10^{-4} mol) were placed in one-side of the H-shaped cell, and pz (2×10^{-4} mol) was placed into the other side of the cell. The CH_3CN crystallization solvent was then slowly filled into the H-shaped cell. Single crystals **1**, **2**, **3**, and **4** were obtained as green needle-like crystals in yields of 40, 42, 38, and 46%, respectively. The crystal stoichiometries were determined by X-ray crystal structural analyses, thermogravimetric measurements, and elemental analyses. The CH_3CN crystallization solvent molecules in the as-grown crystals were easily replaced with H_2O molecules under ambient conditions; therefore, elemental analyses were conducted using the hydrated crystals. Elemental analysis of crystal **1**•1.3H_2O: Calcd for $C_{32}H_{22.66}O_{9.33}N_2F_4Cu_2$: C, 48.80; H, 2.90; N, 3.56. Found: C: 49.01%, H: 2.89%, N: 3.56%. Crystal **2**•3H_2O: Calcd for $C_{32}H_{22}O_{11}N_2F_8Cu_2$: C, 43.20; H, 2.49; N, 3.15. Found: C, 43.43; H, 2.54; N, 3.25. Crystal **3**•0.5H_2O: Calcd for $C_{36}H_{33}O_{8.5}N_2Cu_2$: C, 57.14; H, 4.40; N, 3.70. Found: C, 57.18; H, 4.34; N, 3.89. Crystal **4**•0.5H_2O: Calcd for $C_{32}H_{21}O_{8.5}N_2Cl_4Cu_2$: C, 45.84; H, 2.52; N, 3.34. Found: C, 45.70; H, 2.57; N, 3.38.

X-ray structural analysis. Each single crystal was mounted on a thin polyimide film (MiTeGen MicroMounts) using oil (Hampton Research Parabar 10312). Temperature-dependent crystallographic data (Table 1) were collected for crystals **1**•4CH_3CN and **3**•2CH_3CN **4**•2CH_3CN using a Rigaku RAPID-II diffractometer equipped with a rotating anode fitted with multilayer confocal optics using Cu-Kα (λ = 1.54187 Å) radiation, while that for crystal **2**•4CH_3CN was obtained with a Bruker SMART APEX-II Ultra diffractometer equipped with a rotating anode fitted with a multilayer confocal optic using Mo-Kα (λ = 0.71073 Å) radiation. Calculations were performed using the Crystal Structure software package.[15] Parameters were refined using anisotropic temperature factors, except for the hydrogen atoms. The hydrogen atoms for the disordered pz groups of **2**•4CH_3CN were removed in the structural refinements. The disordered guest CH_3CN molecules for **2** could not be modeled and were treated with the SQUEEZE routine of PLATON.[16]

Thermogravimetry-differential thermal analysis (TG-DTA) and differential scanning calorimetry (DSC) measurements. TG-DTA analyses were conducted using a Rigaku Thermo plus TG8120 thermal analysis station with Al_2O_3 as a reference in the temperature range from 300 to 600 K with a heating rate of 5 K min^{-1} and under N_2. DSC analyses under CO_2 were conducted using a Mettler Toledo DSC 1 STARe system with an empty Al pan as a reference in the temperature range from 170 to 420 K. The scan rate and CO_2 flow rate were 5 K min^{-1} and 60 mL min^{-1}, respectively. Adsorbed H_2O molecules were removed by heating the samples up to 423 K prior to the measurements.

Adsorption measurements. CO_2 adsorption-desorption isotherms (195, 273, and 293 K) were measured with an automatic volumetric adsorption apparatus (BELSORP-max, BEL Japan, Inc). The samples were heated at 373 K under reduced pressure (<10^{-2} Pa) for more than 24 h prior to measurements.

Dielectric measurements. Temperature-dependent dielectric constants under vacuum and CO_2 environment were measured by the two-probe AC impedance method using an impedance/gain-phase analyzer (HP 4194A) at frequencies of 1, 10, 100, and 1000 kHz. A compressed pellet (8 mm diameter) of the sample was placed into the cryostat. Electrical contacts were prepared using gold paste (Tokuriki 8560) to attach 25 μm diameter gold wires. The H_2O molecules in the crystals under ambient conditions were completely removed by keeping the pellets at 373 K and 1 Pa for 24 h prior to measurement. After measurement under vacuum from 200 to 310 K, the pellet samples were again cooled down to 200 K and CO_2 gas adsorption was conducted under a CO_2 pressure of 1.053×10^5 Pa for 24 h. The dielectric constants in the CO_2 environment were measured in the temperature range from 200 to 310 K.

Table 1. Crystal Data, Data Collection, and Reduction Parameter.

	1•4CH_3CN	**2**•4CH_3CN	**3**•2CH_3CN	**4**•2CH_3CN
Formula	$C_{40}H_{32}N_6O_8F_4Cu_2$	$C_{40}H_{28}N_6O_8F_8Cu_2$	$C_{40}H_{38}N_4O_8Cu_2$	$C_{36}H_{26}N_4O_8Cl_4Cu_2$
Formula weight	927.80	999.76	829.85	911.53
Space group	*P*-42$_1$c (#114)	*P*ccn (#56)	*F*dd2 (#43)	*P*2$_1$/n (#14)
a, Å	20.4136(3)	20.2293(4)	19.765(3)	9.7330(2)
b, Å	-	20.5119(4)	38.589(6)	19.3651(6)
c, Å	19.3775(3)	19.3078(3)	9.739(2)	10.3996(2)
β, deg	-	-	-	107.896(1)
V, Å^3	8074.9(2)	8011.6(3)	7428(2)	1865.29(8)
Z	8	8	8	2
T, K	108	108	100	100
D_{calc}, g·cm^{-1}	1.526	1.658	1.484	1.623
μ, cm^{-1}	19.83	21.985	12.043	45.34
Reflections measured	60904	85720	9885	20692
Independent reflections	7357	7327	3922	3408
Reflections used	7357	7327	3922	3408
R_{int}	0.0688	0.1109	0.0219	0.0861
R_1 [a]	0.0583	0.1104	0.0215	0.0820
R_w (F^2) [b]	0.1432	0.3547	0.0556	0.2492
GOF	0.960	1.107	1.031	1.137
Flack Parameter	0.52(5)	-	0.043(9)	-

[a] $R = \Sigma||F_o| - |F_c||/\Sigma|F_o|$ [$I > 2\ \sigma(I)$]. [b] $R_w = (\Sigma\omega(|F_o| - |F_c|)^2/\Sigma\omega F_o^2)^{1/2}$ (all data).

Results and Discussion

Preparation and Crystal Formulas. The preparation, crystal structure, and gas-adsorption properties of one-dimensional coordination polymers of $[Cu(II)_2(BA)_4(pz)]_\infty$ have already been reported.[11] Two Cu(II) ions are bridged by the oxygen atoms of the four BA ligands to form a paddle-wheel type Cu(II) binuclear unit. Each $[Cu(II)_2(BA)_4]$ unit is further coordinated by the axial pz ligand to form a one-dimensional coordination polymer chain of $[Cu(II)_2(BA)_4(pz)]_\infty$. The parallel arrangement of $[Cu(II)_2(BA)_4(pz)]_\infty$ chains within the crystal forms a one-dimensional molecular adsorption space between the polymers, which is utilized as a selective gas adsorption environment. The size and flexibility of the one-dimensional channel are determined by the interchain interactions between BA ligands, so that the chemical design of the BA ligands plays an important role for adjustment of the molecular adsorption properties. Considering this, four types of BA ligand, *m*-FBA, F_2-FBA, *m*-MBA, and *m*-ClBA, were introduced into the Cu(II) binuclear unit to form single crystals of the one-dimensional polymers.

Single crystals of **1**•4CH_3CN, **2**•4CH_3CN, **3**•2CH_3CN, and **4**•2CH_3CN one-dimensional coordination polymers were obtained by a diffusion method with $Cu(II)(AcO)_2$ and the corresponding BA under the slow diffusion of pz molecules in CH_3CN. Crystallization CH_3CN molecules were present in the crystal lattice of the as-grown samples and were easily replaced with H_2O molecules under ambient conditions. Quick hand picking of a single crystal from CH_3CN solution and mounting on the goniometer at 100 K was necessary for the X-ray crystal structural analyses. The atomic coordinates of CH_3CN molecules were confirmed by X-ray crystal structural analyses of crystals **1**, **3**, and **4**; however, that of crystal **2** was not clearly identified from the residual electron densities due to low crystal stability under ambient conditions. However, calculation of the void space using the SQUEEZE program in PLATON suggested four CH_3CN molecules in the crystal, **2**•4CH_3CN. Elemental analyses of the single crystals under ambient conditions corresponded to the hydrated crystal formulas of **1**•1.3H_2O, **2**•3H_2O, **3**•0.5H_2O, and **4**•0.5H_2O, which were consistent with the IR spectra (Figure S1) and TG measurements.

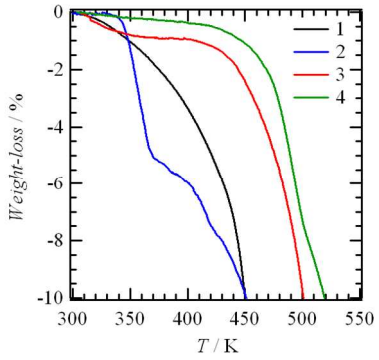

Fig. 1. TG profiles for crystals **1**•1.3H_2O, **2**•3H_2O, **3**•0.5H_2O, and **4**•0.5H_2O under ambient conditions with nitrogen flow.

Figure 1 shows TG profiles for crystals **1**, **2**, **3**, and **4** in the temperature range from 300 to 550 K. The CH_3CN molecules in the as-grown crystals were already replaced with H_2O molecules, so that the weight loss in the TG measurements is associated with the removal of H_2O molecules. A gradual decrease of the sample weight was observed for **1**•1.3H_2O from 300 K, where the calculated weight of 1.3(H_2O) (3.0%) was almost consistent with the weight-loss of 3.36% at 400 K. The TG profile for crystal **1** did not show a clear step of weight loss, which indicates that the **1**•1.3H_2O crystal was not stable at 300 K under the ambient conditions. Crystal **2**•3H_2O was thermally stable in the temperature range from 300 to 350 K, and a step with 5.97% weight loss around 400 K was almost consistent with the calculated weight of 3(H_2O) (6.08%). Although the as-grown **2**•4CH_3CN crystal was quite unstable under ambient conditions, the hydrated crystal of **2**•3H_2O was stable around 300 K. X-ray crystal structural analysis of the **2**•3H_2O single crystal was not successful due to the low crystal quality. The crystal formulas of **3**•0.5H_2O and **4**•0.5H_2O were confirmed by elemental analyses under ambient conditions. The weight of crystal **3**•0.5H_2O was gradually decreased from 300 K and reached a constant weight loss of 1.07% at 400 K, which was consistent with the calculated weight of 0.5(H_2O) molecule (1.19%). The 0.38% weight loss of crystal **4** at 400 K was less than the calculated weight of 0.5(H_2O) molecule (1.07%). In

the TG profiles, the thermal stability of crystals **3**•0.5H_2O and **4**•0.5H_2O were higher than that of crystals **1**•1.3H_2O and **2**•3H_2O.

Molecular Structures. The one-dimensional coordination polymers in single crystals of **1**•4CH_3CN, **2**•4CH_3CN, **3**•2CH_3CN, and **4**•2CH_3CN were determined by X-ray crystal structural analyses and the molecular structures are shown in Figure 2. Two crystallographically independent $[Cu(II)_2(m\text{-}FBA)_4(pz)]_\infty$ and $[Cu(II)_2(2,3\text{-}FBA)_4(pz)]_\infty$ chains (**A**- and **B**-chains) were observed in crystals **1** and **2** (Figures 2a and 2b). Table 2 summarizes the selected structural parameters for each chain and the type of interchain interactions.

The crystal symmetry of **1**•4CH_3CN was tetragonal $P\text{-}42_1c$ with the non-centrosymmetrical and non polar space group. Crystal **1**•4CH_3CN had the twofold symmetry. The two independent **A**- and **B**-chains were elongated along the *c* axis. Although the orientational disorder of the axial pz ligand was not observed in both of the chains, the orientational disorder of F-atoms was observed in one *m*-FBA ligand in the **A**-chain (F1A:F1B pair) and two *m*-FBA ligands in the **B**-chain (F3A:F3B and F4A:F4B pairs). In contrast, no orientational disorder was observed in the F2-site of the **A**-chain. In the **B**-chain, the net dipole moment was cancelled by the alternate arrangement of F3A and F3B sites within the paddle-wheel unit. The same ligand arrangement of F4A and F4B sites within the paddle-wheel unit was observed in the **B**-chain.

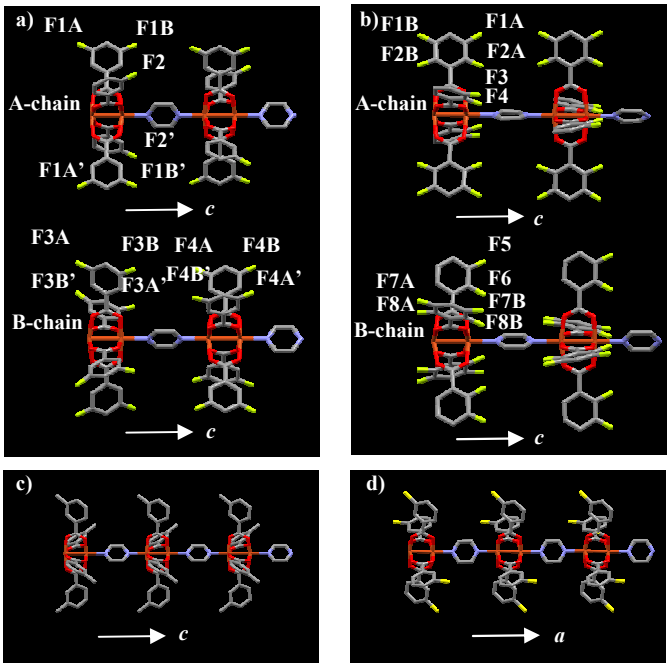

Fig. 2. One-dimensional coordination polymers of a) $[Cu(II)_2(m\text{-}FBA)_4(pz)]_\infty$ in crystal **1**•4CH_3CN, b) $[Cu(II)_2(2,3\text{-}F_2BA)_4(pz)]_\infty$ in crystal **2**•4CH_3CN, c) $[Cu(II)_2(m\text{-}MBA)_4(pz)]_\infty$ in crystal **3**•2CH_3CN, and d) $[Cu(II)_2(m\text{-}ClBA)_4(pz)]_\infty$ in crystal **4**•2CH_3CN. Two crystallographically independent **A**- and **B**-chains were observed in crystals **1** and **2**.

The crystal symmetry of **2**•4CH_3CN was ortholombic *P*ccn with the centric space group. Crystals **2**•4CH_3CN had the imposed symmetry. The crystallization CH_3CN molecules were observed in the residual electron densities with large thermal eliposoide. Two crystallographically independent **A**- and **B**-chains were observed in crystal **2**. Orientational disorder of F-atoms at the 2- and 3-positions was observed for F1A:F1B and F2A:F2B in the **A**-chain and F7A: F8B in the **B**-chain. The 2,3-F_2BA ligands were alternatively arranged within the paddle-wheel unit, which cancelled the net dipole moment of the **A**-chain. However, disordered 2,3-F_2BA ligands were present in the same orientation of the paddle-wheel unit, which generated the net dipole moment of the **B**-chain.

The crystal symmetries of **3**•2CH_3CN and **4**•2CH_3CN were the orthorhombic *F*dd2 and monoclinic $P2_1/n$, respectively. The acentric space group was observed in **3**•2CH_3CN with the polar vector along the *c* axis. Crystals **3**•2CH_3CN and **4**•2CH_3CN had twofold symmetry and inversion symmetry within the unit cell, resepctively. A half unit of $[Cu_2(m\text{-}MBA)_4(pz)]$ in crystal **3**•2CH_3CN and that of $[Cu_2(m\text{-}ClBA)_4(pz)]$ in crystal **4**•2CH_3CN were the crystallographically independent structural units. The four *m*-MBA ligands in the paddle-wheel $[Cu(II)_2(m\text{-}MBA)_4]$ unit were alternatively arranged at the up-down configuration (Figure 2c), whereas the four *m*-ClBA ligands of the $[Cu_2(m\text{-}ClBA)_4]$ unit were arranged in the up-up-down-down configuration (Figure 2d).

Packing Structures of Polymers. The one-dimensional coordination polymers of **1**, **2**, and **3** were arranged along the *c* axis, where each polymer undergoes interchain interaction between the BA ligands within the *ab* plane. In contrast, the polymer chains of **4** were elongated along the *a*-axis. Although the space groups of crystals **1**-**4** were different, bundle-like polymer assemblies were commonly observed. Figure 3 summarizes the packing structures of the one-dimensional coordination polymers of crystals **1**, **3**, and **4**.

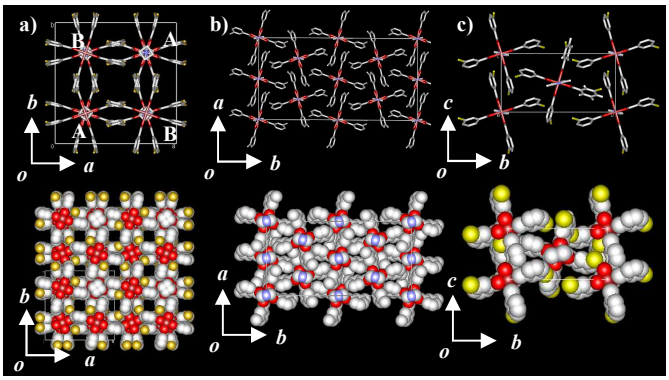

Fig. 3. Packing structures of the one-dimensional coordination polymers in crystals a) **1**•4CH_3CN, b) **3**•2CH_3CN, and c) **4**•2CH_3CN. Lower panels correspond to the CPK representations of the upper panel packing structures. The void spaces between the polymers are occupied by crystallization CH_3CN molecules, which have been omitted from the figures for clarity.

Table 2. Selected structural parameters for crystals **1**-**4**.

Crystal	**1**•4CH_3CN	**2**•4CH_3CN	**3**•2CH_3CN	**4**•2CH_3CN
V_{void}, Å^3 [e]	161	175	76	90
Porosity,%[b]	15.9	17.2	8.18	9.68
Interchain Interaction[c]	4 π-dimer	4 π-dimer	4 vdW	π-dimer +3vdW
d_{plane}, Å [d]	3.60, 3.59	3.60	-	3.43
ϕ, deg [e]	6.20	2.79	51.4	27.0

[a] V_{void} is the void space between the polymers, which was obtained using the SQUEEZE routine of PLATON. [b] The porosity of void spaces in the crystals was determined by ZV_{void}/V. [c] Type and number of interchain interactions of neighboring BA ligands between the polymers. π-Dimer and van der Waals (vdW) interactions were observed. [d] Average interplanar distance of two C_6-planes in π-dimer. [e] ϕ is the dihedral angle of two neighboring BA ligands.

The packing structures of **1** and **2** resemble each other, whereas that of crystal **3** is slightly different from that of crystal **4**. In all of the as-grown crystals, void spaces are observed between the polymer arrangements, which are occupied by the crystallization CH_3CN molecules. In the unit cell of crystal **1**•4CH_3CN (Figure 3a), **A**- and **B**-chains of $[Cu(II)_2(m\text{-}FBA)_4(pz)]_\infty$ are alternatively arranged in the *ab* plane, where the one-dimensional channels between the polymers are along the *c*-axis. The crystallographically independent $[Cu(II)_2(2,3\text{-}F_2BA)_4(pz)]_\infty$ **A**- and **B**-chains of crystal **2** are also alternatively arranged in the *ab* plane, which is the same arrangement as that of crystal **1**. For crystal **2**, the residual electron density map did not indicate the crystallization CH_3CN molecules within the channel. The calculated void space of crystal **2** (V_{void} = 175 Å^3) was almost the same as that of crystal **1**, where four CH_3CN molecules can occupy the channel space. Figures 3b and 3c show the unit cells of crystals 3 and 4 viewed along the *c* and ***a*** axes, respectively. The $[Cu(II)_2(m\text{-}MBA)_4(pz)]_\infty$ and $[Cu(II)_2(m\text{-}ClBA)_4(pz)]_\infty$ chains are elongated along the *c*- and *a*-axis, and each chain is interdigitated within the *ab* and *bc* planes, respectively.

The channel size was increased in the order of **3** (V_{void} = 76 Å^3), **4** (V_{void} = 90 Å^3), **1** (V_{void} = 160 Å^3), and **2** (V_{void} = 176 Å^3). The porosity in the crystals was determined from ZV_{void}/V, and the values for crystals **1**, **2**, **3**, and **4** were 15.9, 17.2, 8.18, and 9.68%, respectively. The intermolecular interactions between the BA ligands of neighboring chains play an important role to determine the channel size. The introduction of the F-group into the BA ligand was effective to increase the channel size. Figure 4 summarizes the observed intermolecular interaction modes between the neighboring BA ligands in crystals **1**-**4**. Two different π-dimer interactions between the neighboring *m*-FBA ligands were observed in crystal **1** with the mean interplanar distances of 3.60 and 3.59 Å, respectively (Figure 4a), which indicates that π-dimer interactions were dominant in the formation of the channel structure. The dipole-dipole interactions of F-groups in the *m*-FBA ligands were also observed in the π-dimer.

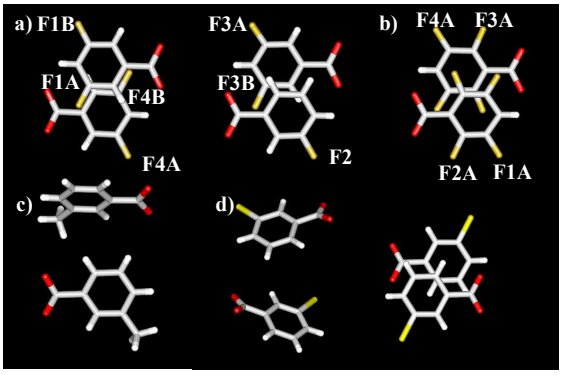

Fig. 4. Intermolecular interaction modes of BA ligands between neighbouring polymers. The π-dimer interactions of a) *m*-FBA ligands in crystal **1** and b) 2,3-F_2BA ligands in crystal **2**. Two different π-dimer interactions were observed in crystal **1**. c) van der Waals interaction of neighbouring *m*-MBA ligands. d) van der Waals interaction (left) and π-dimer interaction with the antiparallel *m*-ClBA arrangement between neighbouring polymers.

Both π-dimer and dipole-dipole interactions were observed in the interchain interaction of crystal **2** (Figure 4b). The average interplanar distance between the two C6-planes of 2,3-F_2BA ligands (d_{plane} = 3.60 Å) was almost the same as those in crystal **1** (d_{plane} = 3.60 and 3.59 Å).

In crystal **3**, the π-π interaction was not observed in the interchain interaction between polymers. The dihedral angle of two neighboring *m*-MBA ligands (ϕ_2) was 51.4°, and van der Waals interaction was observed in the orthogonal arrangement of the *m*-MBA ligands. Both types of interchain interactions, π-dimer and van der Waals, were observed in crystal **4**. Among the four *m*-ClBA ligands in the paddle-wheel unit, one *m*-ClBA ligand formed a π-dimer arrangement with the outer antiparallel arrangement of Cl-groups (right in Figure 4d). The mean interplanar distance of d_{plane} = 3.425 Å was shorter than those of crystal **1**, and the number of π-π interactions was one-third of that in crystal **1**. The other three *m*-ClBA ligands were arranged by van der Waals interaction with a dihedral angle of ϕ_2 = 27.0° between two ligands (left in Figure 4d). The interchain interaction between the polymers was significantly modified by replacement of the BA ligands from *m*-FBA to *m*-ClBA, which partially destroyed the π-dimer arrangements of *m*-FBA ligands and decreased the void space size from 161 Å^3 in crystal **1** to 90 Å^3 in crystal **4**. Gas adsorption occurs in the channels; therefore, the gas adsorption properties of these crystals are dominated by the interchain interactions between BA ligands.

CO_2 Adsorption-Desorption Isotherms. Figure 5 shows CO_2 adsorption-desorption isotherms for crystals **1**-**4** measured at 195 K. There were no adsorption properties for N_2 molecules at 77 K (see Figures S13 in Supporting Information). The number of CO_2 molecules adsorbed per $[Cu(II)_2(R\text{-}BA)_4$•pz] unit (n_{ads}, mol Cu_2 unit) is plotted as a function of the relative CO_2 pressure (P/P_0) from 10^{-5} to 10^0 for the adsorption process and from 10^{-2} to 10^0 for the desorption process. The maximum n_{ads} for crystals **1**, **2**, **3**, and **4** were reached at 3(CO_2), 4(CO_2), 1.5(CO_2), and 3(CO_2), respectively, at P/P_0 = 1, which is much smaller than that expected from the void space based on the X-ray crystal structural analyses. Gated CO_2 adsorption behavior was observed in all crystals. Although the hysteresis behavior of crystal **4** was difficult to confirm at P/P_0 less than ca. 10^{-2} for the desorption process, gated CO_2 adsorption behavior with hysterics was clearly observed for crystals **1**, **2**, and **3**. Such gated CO_2 adsorption processes have been discussed with regard to the structural changes of $[Cu(II)_2(BA)_4$•pz$]_\infty$ polymers and the changes in the assembly structures of each polymer;[11] therefore, the CO_2 adsorption-desorption processes in crystals **1**, **2**, and **3** are dominated by the structural changes of the polymer arrangements.

The CO_2 adsorption-desorption behaviors of crystals **1**, **2**, and **3** are similar, but are different of the two-step CO_2 adsorption observed for crystal **4**. The gradual increase of n_{ads} for crystal **1** was suddenly jumped to around $P/P_0 \sim 10^{-1}$ in the adsorption process, whereas that of crystal **2** was increased significantly around $P/P_0 \sim 10^{-1}$ from n_{ads} ca. 2 to ca. 4 with a large hysteresis for the adsorption and desorption processes. The n_{ads} jump for crystal **3** was observed at $P/P_0 \sim 10^{-2}$ in the adsorption process, and partial hysteresis behavior was observed for the desorption process. The magnitude of n_{ads} at ca. 1.5 at $P/P_0 \sim 10^0$ for crystal **3** was less than half of that for crystals **1** and **2**, which indicates that the CO_2 adsorption ability of crystal **3** is lower than that of crystals **1** and **2**. In contrast, that for crystal **4** was different from those of crystals **1**-**3**. The two-step n_{ads} jumps were observed during the adsorption process at approximately $P/P_0 = 3.3\times10^{-4}$ and 6.2×10^{-4}. After the second n_{ads} jump at $P/P_0 \sim 6.2\times10^{-4}$, a gradual increase of n_{ads} was observed up to $P/P_0 \sim 10^0$ until it reached the n_{ads} maximum of 3(CO_2).

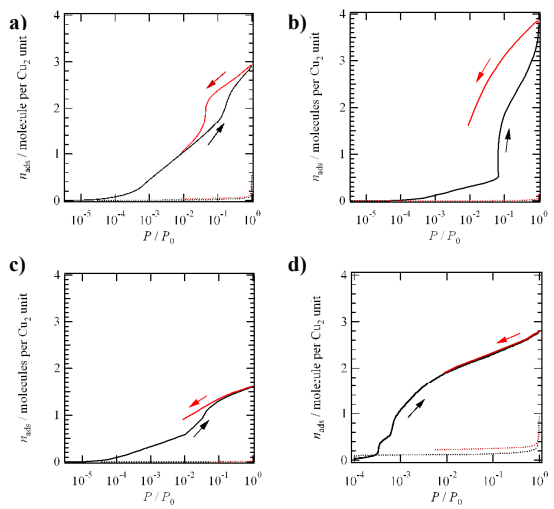

Fig. 5. CO_2 adsorption-desorption isotherms for crystals a) **1**, b) **2**, c) **3**, and d) **4** per $[Cu(II)_2(BA)_4 \cdot (pz)]$ unit at 195 K. The black ($10^{-5} < P/P_0 < 10^0$) and red ($10^0 > P/P_0 > 10^{-2}$) lines represent adsorption and desorption processes, respectively. The dashed lines indicate N_2 adsorption-desorption isotherms for crystals a) **1**, b) **2**, c) **3**, and d) **4** per [Cu(II)2(BA)4•pz] unit at 77 K (see expanded figures of Figures S13).

The n_{ads} jumps and hysteresis behavior in the isotherms are characteristic of a gated adsorption-desorption process in $[Cu(II)_2(R\text{-}BA)_4 \bullet (pz)]_\infty$ crystals, where the size of the void spaces is significantly changed by structural changes in the crystal. The CO_2 adsorption-desorption processes occur in the channel space surrounded by the polymer chains, so that the gated adsorption-desorption process is dominated by the interchain interactions between neighboring BA ligands (Figure 4). The π-dimer interactions in crystals **1** and **2** result in similar gated adsorption-desorption isotherms, where the gate open relative pressures of $P/P_0 \sim 10^{-1}$ are consistent with each other. The channel size of crystal **2** is larger than that of crystal **1**, which results in a larger amount of CO_2 adsorption and larger hysteresis. In contrast, the gate open relative pressure of crystal **3** ($P/P_0 \sim 10^{-2}$) is one order of magnitude lower than that of crystals **1** and **2**, which suggests weaker interchain interaction in crystal **3**; only weak van der Waals interaction between *m*-MBA ligands was observed in crystal **3**, in contrast with the π-dimer interactions in crystals **1** and **2**. The two-step gate open relative pressures at approximately $P/P_0 = 3.3\times10^{-4}$ and 6.2×10^{-4} for crystal **4** were lower than those in crystal **3**, which is consistent with the two types of interchain interactions between *m*-ClBA ligands (π-dimer and van der Waals interactions). One of the four *m*-ClBA ligands formed the π-dimer and the other three ligands underwent van der Waals interaction. Therefore, the two-step gated CO_2 adsorption behavior in crystal **4** is attributed to the two different interchain interactions. Adsorption properties such as the maximum adsorption amount, gate open pressure, multi-step gate behavior, and size of the hysteresis are affected by the interchain interaction between $[Cu(II)_2(R\text{-}BA)_4 \bullet (pz)]_\infty$ polymers, and are therefore adjustable according to the design of the BA ligands.

Dielectric properties under CO_2. The temperature- and frequency-dependent dielectric constants (ε_1) are sensitive to the molecular motions of polar units in the crystals. The two-fold flip-flop motions of BA and pz ligands have been examined in the $[Cu(II)_2(BA)_4(pz)]_\infty$ crystal (**5**) using solid-state ^1H and ^2H NMR spectroscopy.[11] Both the initial and rotated structures of the BA and pz ligands are the same; therefore, no dielectric responses were expected in crystal **5**. The temperature- and frequency-dependent ε_1 for crystals **1**, **2**, **3**, and **4** were evaluated under vacuum and with CO_2 adsorption from 200 to 310 K. The CO_2 molecule has no net dipole moment, so that only the thermal motion and/or fluctuation of the polar ligands can contribute to the dielectric response.

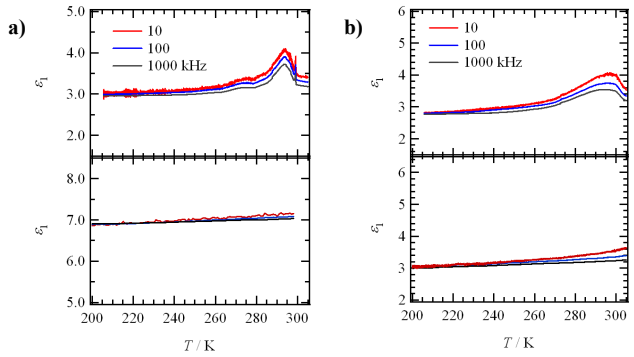

Fig. 6. Temperature- ($200 < T < 310$ K) and frequency-dependent (f = 10, 100, and 1000 kHz) dielectric constants (ε_1) for crystals a) **1** and b) **2**. Pellet samples were measured under vacuum (lower panel) and CO_2 adsorption (upper panel) conditions.

Figures 6a and 6b show the temperature- and frequency-dependent ε_1 for crystals **1** and **2**, respectively, under vacuum and CO_2 conditions. A constant and frequency-independent ε_1 of ca. 7 was observed for crystal **1** under vacuum (lower panel, Figure 6a), which indicates no dielectric response from molecular motion. In contrast, a broad dielectric peak was observed for crystal **1** with CO_2 adsorption around 297 K, where the ε_1 at ca. 4.5 was 1.5 times larger than that measured at 200 K (upper panel, Figure 6a). The dielectric response of crystal **2** under vacuum showed a slight enhancement with temperature, from $\varepsilon_1 \sim 3$ at 200 K to $\varepsilon_1 \sim 3.5$ at 300 K (lower panel, Figure 6b). The low frequency ε_1 enhancement of crystal **2** under vacuum indicates slow molecular motion in the crystal structure of the $[Cu(II)_2(2,3\text{-}F_2BA)_4(pz)]_\infty$ polymers. The larger n_{ads} maximum and hysteresis of crystal **2** than crystal **1** are consistent with a larger and more flexible channel space, and hence, the slight dielectric response. A broad ε_1 peak was observed at 293 K for crystal **2** under CO_2 (upper panel, Figure 6b). The $\varepsilon_1 \sim 4$ at 300 K for crystal **2** under CO_2 is approximately 1.3 times larger than that at 200 K. The ε_1 enhancement for crystal **2** under CO_2 was larger than that in vacuum, which indicates that molecular motion was activated by the presence of CO_2. In contrast, no significant ε_1 enhancements were observed for either crystals **3** or **4** under both vacuum and CO_2 adsorption conditions.

The CO_2 adsorption behavior of crystals **1** and **2** was further evaluated around room temperature to clarify the origin of the dielectric anomalies. Figure 7a shows DSC traces for the heating processes of crystals **1** and **2** under CO_2 flow. When CO_2 desorption from the CO_2 adsorption crystals occurs during the heating process, the DSC traces should show a broad endothermic peak in addition to a flat base line. Almost flat baselines were observed in the high temperature region above 340 K, where the CO_2 molecules have been completely removed from the crystals. The DSC trace for crystal **1** shows the tail of an endothermic peak between 240 and 330 K, which indicates CO_2 desorption from crystal **1** during the heating process. The DSC trace for crystal **2** shows a clear endothermic peak around 290 K, which indicates the desorption of CO_2 from

crystal **2**. The trend of CO_2 desorption for crystals **1** and **2** in this temperature region is reasonably consistent with the dielectric anomalies, which suggests that CO_2 desorption with increasing temperature influences the dielectric responses under CO_2 conditions.

Figure 7b shows the CO_2 adsorption-desorption isotherms for crystals **1** and **2** measured at 273 and 293 K, which are consistent with the CO_2 adsorption behavior at room temperature. One mole of CO_2 molecules was adsorbed in crystal **1** at 273 K, whereas half a mole of CO_2 molecules was adsorbed at 293 K. Although the amount of CO_2 adsorption in crystal **2** was almost half that of crystal **1**, CO_2 adsorption was observed around room temperature. The DSC traces and CO_2 adsorption-desorption isotherms indicate that CO_2 adsorption-desorption processes in crystals **1** and **2** are possible under a CO_2 environment around room temperature and could thus be responsible for the dielectric anomalies under a CO_2 environment.

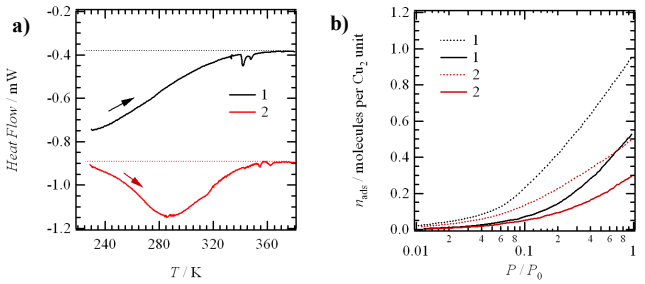

Fig. 7. CO_2 gas adsorption properties for crystals **1** and **2** around room temperatures. a) DSC traces for crystals **1** and **2** under CO_2 flow with a scan rate of 5 K min^{-1}. b) CO_2 desorption curves for crystals **1** (black) and **2** (red) at 273 (dashed line) and 293 K (solid line).

Crystals **1** and **2** exhibited CO_2 desorption processes with increasing temperature, which activated the thermal motion of polar *m*-FBA and 2,3-F_2BA ligands, and hence the dielectric responses. The small magnitude of dielectric response was not consistent with the two-fold flip-flop motion of polar BA ligands; therefore, the small amplitude fluctuations of BA ligands contributed to the dielectric anomalies of crystals **1** and **2**. Although gated CO_2 adsorption-desorption isotherms were observed for crystals **3** and **4**, no ε_1 anomalies were confirmed under a CO_2 environment (see Figure S10). The size of the CH_3- and Cl-groups in the *m*-MBA and *m*-ClBA ligands are larger than the F-group (van der Waals radius of CH_3-, Cl-, and F-groups are 2.00, 1.80 and 1.35 Å, respectively).[17] The large size polar ligands in crystals **3** and **4** are strongly interdigitated to each other without motional freedom, which is consistent with the lack of orientational disorder in these crystals.

Conclusion

Four new single crystals of **1**•4CH_3CN, **2**•4CH_3CN, **3**•2CH_3CN, and **4**•2CH_3CN were prepared to examine the CO_2 adsorption-desorption properties coupled with dielectric response. The polar ligands of *m*-FBA, 2,3-F_2BA, *m*-MBA, and *m*-ClBA were introduced into the Cu(II) binuclear unit as bridging ligands between two Cu(II) sites. Although one-dimensional coordination polymers were observed as a common structure of crystals **1**-**4**, the interchain interactions were different. Both π-dimer and dipole-dipole interactions were observed in the *m*-FBA and 2,3-F_2BA ligands of crystals **1** and **2**, which resulted in similar gated CO_2 adsorption-desorption properties. The maximum amounts of CO_2 adsorption in crystals **1** and **2** at 195 K were reached at 3(CO_2) and 4(CO_2) per [Cu(II)$_2$(*R*-BA)$_4$(pz)] unit, respectively. It should be noted that the CO_2 adsorption of crystals **1** and **2** was observed at room temperature, where the dielectric anomalies were observed. The polar BA ligands bearing fluorine groups were more responsive to polar CO_2 and H_2O molecules. The interchain interactions of *m*-MBA and *m*-ClBA ligands were dominated by van der Waals interactions, and the maximum amounts of CO_2 adsorption and gate pressures of crystals **3** and **4** were smaller than those of crystals **1** and **2**, due to their smaller channel sizes. The polar BA ligands bearing F-groups were effective to increase the CO_2 adsorption ability and the dielectric responses around 300 K of crystals **1** and **2** were associated with desorption processes of CO_2 molecules from the crystals under a CO_2 environment. The elimination of CO_2 molecules from the channels gradually modified the dynamic environment of polar *m*-FBA and 2,3-F_2BA ligands. Further design of polar bridging and axial ligands to achieve the crystalline space for molecular rotation will realize the potential for the design of dielectric materials that are responsive to external stimuli such as molecular adsorption.

Acknowledgement

This work was supported by a Grant-in-Aid for Science Research from the Ministry of Education, Culture, Sports, Science, and Technology of Japan, and by Management Expenses Grants for National Universities of Japan and a Grant-in-Aid for Japan Society for the Promotion of Science (JSPS) Fellows (No. 259150).

Notes and references

[a] Graduate School of Engineering, Tohoku University, Sendai 980-8579, Japan.
[b] Institute of Multidisciplinary Research for Advanced Materials (IMRAM), Tohoku University, 2-1-1 Katahira, Aoba-ku, Sendai 980-8577, Japan. Fax: (+81)22-217-5655, E-mail: akuta@tagen.tohoku.ac.jp
[c] Research Institute for Electronic Science, Hokkaido University, Sapporo 001-0020, Japan.
[d] Faculty of Science, Hokkaido University, Sapporo 060-0810, Japan.

† The atomic numbering scheme, structural analysis of **1**-**4**, calculated structure of potential energy curves, IR spectra, and UV-vis-NIR spectra for KBr pellets. X-ray single crystal analyses; CCDC-973257 (**1**•4CH_3CN), CCDC-973258 (**2**•4CH_3CN), CCDC-973258 (**3**•2CH_3CN), and CCDC-973260 (**4**•2CH_3CN) contain the supplementary crystallographic data for this paper. These data can be obtained free of charge from The Cambridge Crystallographic Data Centre via www.ccdc.cam.ac.uk/data_request/cif."

1 (*a*) S. Kitagawa, R. Kitaura, S. Noro, *Angew. Chem. Int. Ed.* 2004, **43**, 2334; (*b*) J. -R. Li, J. Ryan R. J. Kuppler, H. -C. Zhou, *Chem. Soc. Rev.*, 2009, **38**, 1477; (*c*) D. M. Dybtsev, H. Chun S. H. Yoon, D. Kim. K. Kim, *J. Am. Chem. Soc.* 2004, **126**, 32; (*d*) M. Dinca, J. R. Long. *J. Am. Chem. Soc.* 2005, **127**, 9376; (*e*) B. Chen, S. Ma, F. Zapata, F. R. Fronczek, E. B. Lobkovsky, H. -C. Zhou, *Inorg. Chem.* 2007, **46**, 1233; (*f*) J. An, S. J. Geib, N. L. Rosi, *J. Am. Chem. Soc.* 2010, **132**, 38.

2 (*a*) J. Y. Lee, O. K. Farha, J. Roberts, K. A. Scheidt, S. B. T. Nguyen, J. T. Hupp, *Chem. Soc. Rev.* 2009, **38**, 1450; (*b*) L. Ma, C. Abney, W. Lin, *Chem. Soc. Rev.* 2009, **38**, 1248; (*c*) C. -D. Wu, A. Hu, L. Zhang, W. Lin, *J. Am. Chem. Soc.* 2005, **127**, 8940; (*d*) J. S. Seo, D.

Whang, H. Lee, S. I. Jun, J. Oh, Y. J. Jeon, K. Kim, *Nature* 2000, **404**, 982.

3 (*a*) H. Kitagawa, Y. Nagao, M. Fujishima, R. Ikeda, S. Kanda, *Inorg. Chem. Commun.* 2003, **6**, 346; (*b*) M. Sadakiyo, T. Yamada, H.; Kitagawa, *J. Am. Chem. Soc.* 2009, **131**, 9906; (*c*) J. M. Taylor, R. K. Mah, I. L. Moudrakovski, C. I. Ratcliffe, R. Vaidhyanathan, G. K. H. Shimizu, *J. Am. Chem. Soc.* 2010, **132**, 14055; (*d*) S. Bureekaew, S. Horike, M. Higuchi, M. Mizuno, T. Kawamura, D. Tanaka, N. Yanai, S. Kitagawa, *Nat. Mater.* 2009, **8**, 831.

4 (*a*) P. Lin, R. A. Henderson, R. W. Harrington, W. Clegg, C. -D. Wu, X. -T. Wu, *Inorg. Chem.* 2004, **43**, 181; (*b*) S. Q. Liu, T. Kuroda-Sowa, H. Konaka, Y. Suenaga, M. Maekawa, T. Mizutani, G. L. Ning, M. Munakata, *Inorg. Chem.* 2005, **44**, 1031; (*c*) S. Delgado, M. P. J. Sanz, J. L. Priego, R. Jimenez-Aparicio, C. J. Gomez-Garcia, F. Zamora, *Inorg. Chem.* 2008, **47**, 9128; (*d*) Y. -B. Dong, T. Sun, j. -P. Ma, X. -X. Zhao, R. -Q. Huang, *Inorg. Chem.* 2006, **45**, 10613.

5 (*a*) H. Miyasaka, M. Julve, M. Yamashita, R. Clérac, *Inorg. Chem.* 2009, **48**, 3420; (*b*) S. Noro, H. Miyasaka, S. Kitagawa, T. Wada, T. Okubo, M. Yamashita, T. Mitani, *Inorg. Chem.* 2005, **44**, 133; (*c*) N. Re, E. Gallo, C. Floriani, H. Miyasaka, N. Matsumoto, *Inorg. Chem.* 1996, **35**, 6004; (*d*) L. Li, Z. Liu, S. S. Turner, D. Liao, Z. Jiang, S. Yan, *Eur. J. Inorg. Chem*. 2003, **1**, 62; (*e*) C. Coulon, H. Miyasaka, R. Clérac, *Struct. Bonding (Berlin)* 2006, **122**, 163.

6 (*a*) B. Sui, W. Zhao, G. Ma, T. Okamura, J. Fan, Y. -Z. Li, S. -H. Tang, E. -Y. Sun, N. Ueyama, *J. Mater. Chem.* 2004, **14**, 1631; (*b*) L. Li, Y. L. Song, H. W. Hou, Y. T. Fan, Y. Zhu, *Euro. J. Inorg. Chem.* 2005, **16**, 3238; (*c*) I. Ledoux, J. Zyss, *Pure Appl. Opt.* **1996**, *5*, 603; d) Y. Iwasa, E. Funatsu, T. Hasegawa, T. Koda, M. Yamashita, *Appl. Phys. Lett.* 1991, **59**, 2219.

7 (*a*) C. G. Claessens U. Hahn T. Torres *Chem. Rec*. 2008, **8**, 7; (*b*) S. Venkatachalam, K. V. C. Rao, P. T. Manoharan, *Polym. Sci. Part B Polym. Phys.* 1994, **32**, 37; (*c*) S. M. Palmer, J. M. Stanton, B. M. Hoffman, J. A. Ibers, J. A. *Inorg. Chem*. 1986, **25**, 2296.

8 (*a*) N. Robertson, L. Cronin, *Coord. Chem. Rev.* 2002, **227**, 93; (*b*) P. Cassoux, L. Valade, H. Kobayashi, A. Kobayashi, R. A. Clark, A. E. Underhill, *Coord. Chem. Rev.* 1991, **110**, 115; (*c*) T. Nakamura, T. Akutagawa, *Coord. Chem. Rev*. 2000, **198**, 297; (*d*) A. E. Pullen, R. -M. Olk, *Coord. Chem. Rev*. 1999, **188**, 211; (*e*) E. Canadell, E. *Coord. Chem. Rev*. 1999, **186**, 629.

9 (*a*) H. -L. Sun, Z. -M. Wang, S. Gao, *Coord. Chem. Rev.* 2010, **254**, 1081; (*b*) A. Caneschi, D. Gatteschi, N. Lalioti, C. Sangregorio, R. Sessoli, G. Venturi, A. Vindigni, A. Rettori, M. G. Pini, M. A. Novak, *Angew. Chem. Int. Ed.* 2001, **40**, 1760; (*c*) R. Clérac, H. Miyasaka, M. Yamashita, C. Coulon, *J. Am. Chem. Soc.* 2002, **124**, 12837; (*d*) S. W. Choi, H. Y. Kwak, J. H. Yoon, H. C. Kim, E. K. Koh, C. S. Hong, *Inorg. Chem.* 2008, **47**, 10214.

10 C. Coulon, S. Flandrois, P. Delhaes, C. Hauw, P. Dupuis, *Phys. Rev. B.* 1981, **23**, 2850.

11 (a) S. Takamizawa, E. Nakata, T. Akatsuka, R. Miyake Y. Kakizaki, H. Takeuchi, G. Maruta, S. Takeda, S. *J. Am. Chem. Soc.* 2010, **132**, 3783; (*b*) S. Takamizawa, E. Nakata, R. Miyake, *Dalton Trans.* 2009, 1752; (*c*) S. Takamizawa, E. Nakata, T. Akatsuka, C. Kachi-Terajima, R. Miyake, *J. Am. Chem. Soc.* 2008, **130**, 17882; (*d*) S. Takamizawa, T. Saito, T. Akatsuka, E. Nakata, *Inorg. Chem.*, 2005, **44**, 1421.

12 (*a*) S. Nishihara, T. Akutagawa, D. Sato, S. Takeda, S. Noro, T. Nakamura, *Chem. Asian J.* 2007, **2**, 1983; (*b*) T. Akutagawa, D. Sato, H. Koshinaka, M. Aonuma, S. Noro, S. Takeda, T. Nakamura, *Inorg. Chem*. 2008, **47**, 5951; (c) T. Akutagawa, T. Nakamura, *Dalton Trans.* 2008, 6335.

13 T. Akutagawa, H. Koshinaka, D. Sato, S. Takeda, H. Takahashi, R. Kumai, Y. Tokura, T. Nakamura, *Nat. Mater.* 2009, **8**, 342.

14 Q. Ye, K. Takahashi, N. Hoshino, T. Kikuchi, T. Akutagawa, S. Noro, S. Takeda, T. Nakamura, T. *Chem. Eur. J.* 2011, **17**, 14442.

15 (*a*) Crystal structure: single-crystal structure analysis software. Ver. 4.0.1, 2010. Rigaku Corporation and Molecular Structure Corporation; (*b*) G. Sheldrick, M., *SHELX97 Programs for Crystal Structure Analysis*, Universitat Gçttingen, Gçttingen, Germany, 1998; (*c*) SIR2008: M. C. Burla, R. Caliandro, M. Camalli, B. Carrozzini, G. L. Cascarano, L. De Caro, C. Giacovazzo, G. Polidori, D. Siliqi, R. Spagna, *J. Appl. Crystallogr.* 2007, **40**, 609.

16 A. L. Spek, *J. Appl. Crystallogr.* 2003, **36**, 7.

17 C. Raymond, in *Physical Chemistry for the Chemical and Biological Sciences*, University Science Books, 2000, pp. 681.

Graphical Abstract

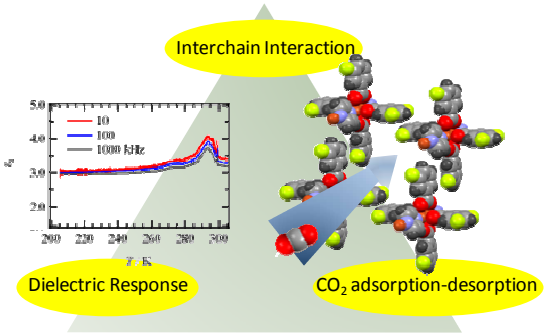

Relationship between the interchain interactions and CO_2 gas adsorption-desorption properties, and dielectric responses under CO_2 desorbed condition.